Effect of sequential release of sirolimus and rosuvastatin using silk fibroin microneedle to prevent intimal hyperplasia

Eui Hwa Jang

The Graduate School
Yonsei University
Graduate program in biomedical engineering

Effect of sequential release of sirolimus and rosuvastatin using silk fibroin microneedle to prevent intimal hyperplasia

Directed by Professor: Young-Nam Youn

The Doctoral Dissertation submitted to
the Department of Medicine,
the Graduate School of Yonsei University
in partial fulfillment of the requirements
for the degree of Doctor of Philosophy

Eui Hwa Jang

December 2022

This certifies that the Doctoral Dissertation

of Eui Hwa Jang is approved.

Thesis Supervisor: Young-Nam Youn

Thesis Committee Member #1: Jae-Kwang Shim

Thesis Committee Member #2: Sang-Hak Lee

Thesis Committee Member #3: Jung-Sun Kim

Thesis Committee Member #4: Won Hyoung Ryu

The Graduate School
Yonsei University
December 2022

ACKNOWLEDGEMENT

Many people have contributed to make my Ph.D. program possible and now it is a great pleasure to convey my deepest gratitude to them all.

First of all, I would like to thank my dissertation adviser Prof. Young-Nam Youn, who has been an invaluable mentor and a guide throughout the program. I have learned many important life lessons from Prof. Youn that will undoubtedly help me find the successful path in my career. I will always cherish all that I have learned from him. Also, I would like to thank my dissertation committee members, Prof. Jae-Kwang Shim, Prof. Sang-Hak Lee, Prof. Jung-Sun Kim and Prof. Won Hyoung Ryu, for their valuable comments and suggestions.

I would like to express my special thanks to our lab members, Jung-Hwan Kim, Hyo-Hyun Kim, and Ji-yeon Ryu, for being a good friend and supporter. The time we spent together will remain in my memory forever.

Last but not the least, I would like to express my heartfelt thanks to my family for their love and endless encouragement.

Eui Hwa Jang

December 2022

TABLE OF CONTENTS

LIST OF FIGURES

LIST OF TABLES

ABBREVIATIONS

DDS	Drug Delivery System
ECM	Extracellular Matrix
HMG-CoA	hydroxymethylglutaryl-coenzyme
IH	Intimal Hyperplasia
IEL	Internal Elastic Lamina
LC–MS/MS	Liquid Chromatography-Tandem Mass Spectrometry
mTOR	Mechanistic Target of Rapamycin
MN	Micorneedle
NF-κB	Nuclear Factor kappa B
PRP	Platelet-rich plasma
SF	Silkfibroin
TGF-β	Transforming Growth Factor- β
VSMC	Vascular Smooth Muscle Cell
YAP	Yes-associated Protein
NI	Neo-Intima

ABSTRACT

Effect of sequential release of sirolimus and rosuvastatin using silk fibroin microneedle to prevent intimal hyperplasia

Eui Hwa Jang

Graduate program in Graduate Program of biomedical engineering

The Graduate School, Yonsei University

(Directed by Professor Young-Nam Youn)

Intimal hyperplasia (IH) is a major cause of vascular restenosis after bypass surgery, which progresses as a series of processes from the acute to chronic stage in response to endothelial damage during bypass grafting. A pharmacological approach is required to understand the key signalling pathways at each stage to prevent IH. A strategic localized drug delivery system that reflects the pathophysiology of IH and minimizes systemic side effects is necessary in addition to systemic therapeutic approaches using oral or

intravenous drugs. In this study, the sequential release of sirolimus, a mechanistic target of rapamycin (mTOR) inhibitor, and statin, an HMG-COA inhibitor, was realized as a silk fibroin-based microneedle device *in vivo*. The released sirolimus in the acute stage reduced vascular smooth muscle cell (VSMC) proliferation and vascular fibrosis through transforming growth factor (TGF)-beta/mTOR inhibition. Furthermore, rosuvastatin, which was continuously released from the acute to chronic stage, reduced vascular stiffness and apoptosis through TGF-beta/Yes-associated protein inactivation. The sequential release of sirolimus and rosuvastatin confirmed the synergistic treatment effects on vascular inflammation, autophagy, VSMC proliferation, and extracellular matrix degradation remodeling through inhibition of the mTOR/nuclear factor kappa B pathway. These results demonstrate the therapeutic effect on preventing restenosis with sufficient vascular elasticity and significantly reduced vascular fiber density of the neointima in response to endothelial damage. We also confirmed the safety of drug toxicity by delivering the drug to the target lesion rather than by systemic diffusion. Thus, the study suggests a promising strategy for treating coronary artery disease in patients with underlying conditions such as diabetes, hypertension, and hyperlipidemia through localized drug delivery of customized drug combinations.

Keywords: intimal hyperplasia, bypass surgery, microneedle, silk fibroin, localized drug delive

Effect of sequential release of sirolimus and rosuvastatin using silk fibroin microneedle to prevent intimal hyperplasia

Eui Hwa Jang

Graduate program in Graduate Program of biomedical engineering

The Graduate School, Yonsei University

(Directed by Professor Young-Nam Youn)

I. INTRODUCTION

Coronary artery obstructive disease generally occurs due to atherosclerosis, which is the leading cause of mortality worldwide. Coronary artery bypass grafting is considered a clinical treatment for revascularization in more severe or acute cases [1,2].

However, restenosis has been reported in up to 40% of cases within 5 years of bypass grafting, and patients with restenosis experience myocardial infarction, sudden death, or reoperation. Although the preservation of grafted vessels is essential for long-term success,

the lack of an acceptable alternative makes it dependent on the systemic administration of compounds in clinical practice [3-6].

Restenosis is a major complication of long-term patency after revascularization, and its pathophysiology is intricate and not fully understood. In contrast to vascular remodeling caused by atherosclerosis, it is interpreted as a maladaptive response to endothelial layer damage during bypass grafting. Restenosis primarily arises from neointimal hyperplasia (IH) due to platelet aggregation, inflammation, vascular smooth muscle cell (VSMC) proliferation, phenotypic switch, and extracellular matrix (ECM) deposition, which contribute to restenosis over time after an endothelial layer injury [7-9]. In particular, myofibroblasts differentiated through mechanical or biochemical simulation are the majority of cells in restenotic lesions and contribute to vascular restenosis by inducing vascular fibrosis [10,11].

To prevent IH, a perivascular drug delivery system (DDS) for localized delivery through diffusion of the loaded target drug from the adventitial layer into the tunica medial layer while preventing de-endothelium is necessary [6]. The development and abundant preclinical results of perivascular devices using various shapes and materials, such as the unimolecular micelle/triblock gel hybrid system, poly(ε-caprolactone) sheath, and external stents, have been reported over the last 25 years. However, most strategies fail to meet expectations in clinical practice due to physiological differences between the experimental models and clinical conditions and poor reflection of time-dependent pathophysiological changes after vascular injury. Improving the efficacy of these drug-loaded perivascular devices requires

the selection of effective compounds with a system design reflecting the pathophysiology (acute to chronic stage) of IH [12-15].

Sirolimus is a well-known local DDS, which inhibits VSMC proliferation by interacting with a mechanistic target of rapamycin (mTOR) to block the G1-to-S phase transition of the cell cycle. Several DDSs, such as *Selution SLR*™ and *MagicTouch*™, have been widely applied in clinical practice as breakthrough devices and have been approved by the FDA. However, potency was reported to decrease from 95.1% at 3 months to 44.4% at 12 months, unlike the preclinical results [16,17]. This observation suggests that additional drug elution may be required in the intermediate process, as well as inhibition of inflammation and VSMC proliferation through interaction with the mTOR pathway. However, applications that regulate and release two or more drugs from a single device are yet to be reported. Moreover, the current treatment guidelines recommend high-dose statin therapy, such as inhibiting hydroxymethylglutaryl-coenzyme (HMG-CoA) reductase, with the administration of antiplatelet drugs after DDS application. In particular, numerous clinical trials have provided evidence that high-dose statin therapy is effective for IH as an independent pleiotropic effect, including anti-inflammatory effects, endothelial function improvement, and antioxidant activity from the hyperacute to chronic stage [18-21]. Although high-dose statin therapy is reportedly effective in patients with underlying diseases such as exertional angina, heart failure, diabetes, left ventricular dysfunction, and chronic kidney disease, its efficiency in patients with stable coronary artery disease is uncertain. Additionally, statin therapy has the most common complaints, including statin-associated

muscle symptoms, hepatotoxicity, and renal toxicity, limiting the dosage and duration of statins [21-23]. Moreover, no clinical trials have evaluated the effect of statins on restenosis using a perivascular device.

Based on these current clinical results, we investigated the efficacy of perivascular application of a systematic microneedle device that induces the sequential release of sirolimus and rosuvastatin in the intensive treatment of localized vessels that minimizes the systemic side effects of drugs in a rabbit model (Figure 1).

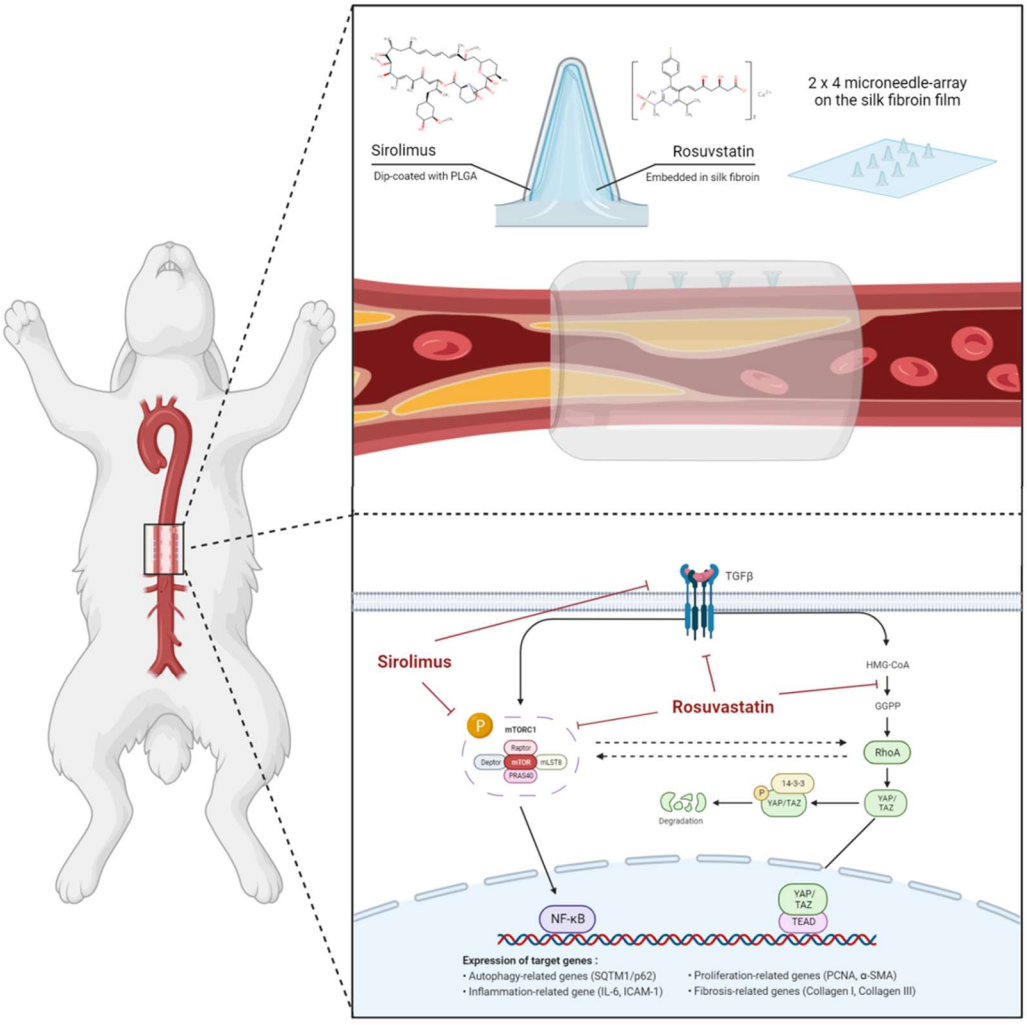

Figure 1. Schematic illustration of the treatment strategy using a silk fibroin-based microneedle device with programmable release of sirolimus (a transforming growth factor beta (TGF-β inhibitor) and a statin (an hydroxymethylglutaryl-coenzyme (HMG-CoA) inhibitor) in the injured abdominal aorta of the rabbit model.

II. MATERIALS AND METHODS

1. Fabrication and surface characterization of the MN devices

To prepare porous silk, 2.3 mL of aqueous silk solution (6.5%, w/w) was poured into a 60-mm Petri dish and frozen for 1 h. After freeze-drying for 1 d, the porous silk wrap was cut and treated with 100% EtOH for 1 min for crystallization. After several washes in deionized (DI) water, a highly porous silk warp with a width and thickness of 10 mm and 400 μm, respectively, was fabricated. Negative polydimethylsiloxane MN molds with a height and aspect ratio of 640 μm and 1.6, respectively, were prepared using Si MN masters [24]. To prepare a 2-μg rosuvastatin-embedded silk MN, 450 mg of rosuvastatin (PHR1928, Sigma-Aldrich, USA) was dissolved in 10 mL of dimethyl sulfoxide (DMSO) for 12 h and homogeneously mixed with an aqueous silk solution at a volume ratio of 1:9. Subsequently, the statin-silk formulation was centrifuged on the negative MN molds for 5 min using an ultracentrifuge (DT5-2B, Beijing Era Beili Centrifuge Co., Ltd., China). The residue of the drug solution in the mold was cleaned by doctor-blading and dried for 30 min. After one more repeated step, the Rosuvastatin-embedded silk MN was transferred to the silk wrap, which was performed according to our previous study [25]. Finally, 1 μg of sirolimus (rapamycin, R-5000, LC Laboratories, MA, USA) was dip-coated onto the rosuvastatin-embedded MNs using a homogeneously mixed drug formulation (weight ratio of 3:1:0.33 = DMSO:PLGA 50/50:sirolimus). A silk MN wrap with sirolimus-coated and rosuvastatin-embedded 2 × 4 silk MNs was then fabricated on a highly flexible and porous silk wrap.

For further *in vivo* studies, each silk MN wrap was placed on a clean bench for 30 min and sterilized by UV.

2. Animals and comparative animal study group

Twenty male New Zealand White rabbits weighing between 3.0 and 4.0 kg were used in this study and reared in the same care according to the "Guide for the Care and Use of Laboratory Animals (National Research Council, USA)." The study protocol was approved by the Institutional Animal Care and Use Committee of the Yonsei University Health System (IACACN No. 2020-0206).

All experimental rabbits were injured by denudation of the endothelium using a balloon catheter and divided into four groups to investigate the efficacy of reducing IH: B-MN group (bare MN without drug; N = 5), S-MN group (1 μg of sirolimus dip-coated; N = 5), R-MN group (2 μg of rosuvastatin embedded; N = 5), and SR-MN group (1 μg of sirolimus dip-coated with 2 μg of rosuvastatin embedded; N = 5).

3. Induced intimal hyperplasia through denudation of endothelium and applications

All procedures, including surgery, sonography, specimen extraction, and sacrifice, were performed under general anesthesia with zoletil (10 mg/kg, intramuscular), rompun (5 mg/kg, intramuscular), and isoflurane (1.5%–2.0%, inhalation). A deendothelialized artery model was generated as a balloon injury three times using a 2 F Fogarty® embolectomy catheter (120602F, Edwards Lifesciences, CA, USA) in the abdominal aorta from the

femoral artery. The MN devices were carefully wrapped around the external surface of the injured abdominal aorta and fixed using a surgical clip (LIGACLIP®, Titanium Medium, Mexico) to fit the individual aortic diameter measured by ultrasonography before surgery. Heparin sodium (100 U/kg, Hanlim, Seoul, Korea) was administered immediately before balloon injury to prevent acute thrombosis, and aspirin (100 mg/day, Bayer Korea, Seoul, Korea) was administered for 4 weeks after surgery.

4. Evaluation of blood and tissue compatibility

Whole blood samples from a normal healthy rabbit were collected into ethylenediaminetetraacetic acid (EDTA) for hemocompatibility. Platelet-rich plasma (PRP) was obtained by double centrifugation at 3000 × g for 5 min and 700 × g for 15 min [26]. After collection, 350 μL of PRP with MN devices was placed in a 24-well plate and incubated at 37 °C for 2 h. The morphology of the adhered platelets on the surface of the MNs was studied by scanning electron microscopy (SEM, IT-500HR), after washing with phosphate buffered saline and fixing with 2.5% glutaraldehyde, dehydrating, and gold spraying. Hemolysis experiments were performed as described by Yang et al. with minor modifications[27]. Briefly, 4 mL of whole blood was placed in 5 mL of 0.9% NaCl solution, centrifuged at 1500 rpm for 15 min, and red blood cells (RBC) were collected. All samples were then placed in a 24-well plate with 40 μL of RBC and 960 μL of 0.9% NaCl, and the plates were incubated at 37 °C for 1 h. Subsequently, the solutions were placed in centrifuge tubes and centrifuged at 3000 rpm for 15 min. Finally, the absorbance at 540 nm was

measured using a spectrophotometer (Soft Max, Molecular Devices, Sunnyvale, CA). Hemolysis ability was quantified as the percentage reduction in absorbance using Triton X-100 and 0.9% NaCl as positive and negative controls, respectively.

The histological biocompatibility of the MN mesh was detected by implantation in a rabbit model by wrapping around the dissected bilateral carotid artery under surgical conditions. The sham, control, B-MN, and SR-MN groups were prepared for analysis using a cardiovascular pledget (TFE polymer, #517717, J&J Healthcare System). Three vessels were implanted in each group for 4 weeks and analyzed using hematoxylin and eosin (H&E) staining.

5. *In vivo* drug release analysis

MN devices were applied to the abdominal tissues of 15 rabbits to identify the sirolimus and rosuvastatin released from the tissue and blood. On days 7, 14, and 28 after application, five animals at each time point were sacrificed, and the abdominal aortas were harvested. Subsequently, 5 mL of whole blood was collected in EDTA tubes after 1, 3, 7, 14, and 28th day of follow-up. Blood samples were stored at -80 °C until drug determination.

Sirolimus and rosuvastatin levels were determined by high-performance liquid chromatography (HPLC, UltiMate^{TM} 3000, Thermo Fisher Scientific, USA) coupled with a Q-Orbitrap mass spectrometer (Q-ExactiveTM Plus, Thermo Fisher Scientific, USA). The separation was achieved using an Acquity UPLCBEH C18 column (100 × 2.1 mm, 1.7 μm, Waters, Milford, MA, USA). The mobile phase consisted of 6.5 mM ammonium

bicarbonate in distilled water (A) and 6.5 mM ammonium bicarbonate acetonitrile (B) as eluents at a flow rate of 0.40 mL/min with the following gradient: 0–2 min, 10% B; 2–8 min, 100% B; 8–12 min, 100% B; 12–12.5 min, 10% B; 12.5–15 min, 10% B. The injection volume was 10 μL, and the oven temperature was set to 40 °C. Selected reaction monitoring transitions of *m/z* 912.54, 480.16, and 790.47 were applied for sirolimus, rosuvastatin, and ascomycin (internal standard), respectively. Mass data and data analysis were acquired using the Thermo software.

6. Evaluation of local arterial stiffness by Doppler ultrasonography

A point defined as a portion 1 cm away from the injured abdominal aorta in a longitudinal view with an ultrasound incident angle of < 60 °was measured. Using remote palpation conducted shear waves through ultrasonography (S8Exp, SonoScape, China), pulse wave velocity (PWV), peak systolic velocity (PSV), and pulsatility index (PI) were measured for the aortic function index, and the circumferential strain (Circ strain), distensibility (DC), compliance (CC), and Young's modulus were calculated to evaluate the vascular pathological situation. The vascular pathological situation is defined as follows:

$$\text{Circ strain} = \frac{\Delta D}{D} \times 100,\ \text{DC} = \frac{\Delta A/A}{\Delta P},\ \text{PWV} = \sqrt{\frac{1}{DC}},\ \text{CC} = \frac{\Delta A}{\Delta P},\ \text{Y} = \frac{D}{h} \times \frac{1}{DC}$$

where A is the surface area of the lumen, ΔA is the change in the transverse section of the vessel between diastole and systole, ΔP is the change in pressure between diastole and systole, D is the diastolic diameter, ΔD is the change in diameter between diastole and systole, and h is the thickness of the vessel wall.

7. Analysis of histopathological characteristics

Histopathological characteristics were evaluated and assessed by H&E, Van Gieson (VG), Masson's trichrome (MT), Picrosirius red (PSR), and TUNEL staining. All extracted samples were cross-sectioned (5 μm thick) from the paraffinized blocks, de-paraffinized in xylene, and dehydrated. The structure of each histological section was manually identified using an Olympus microscope (BX53), and the area of each blood vessel layer was measured using the NIH Image J software in a blinded manner. To assess the narrowing of the vessel lumen and NI formation and normalize the influence of the size of the blood vessel, the NI/media and adventitia/media ratios are defined as follows:

$$NI\ formation = \frac{neointimal\ area}{neointimal\ area + luminal\ area} \times 100\ (\%)$$

$$Ratio\ of\ NI\ /\ Media = \frac{neointimal\ area}{media\ area} \times 100\ (\%)$$

$$Ratio\ of\ Adventitia\ /\ Media = \frac{Adventitia\ area}{media\ area} \times 100\ (\%)$$

The internal elastic lamina (IEL) defect was analyzed by calculating the loss area as a percentage of the whole IEL in the vessel wall using VG staining. Fibrosis was calculated by automatically measuring the integrated density at 100× magnification on an average of four sections per MT staining. Collagen fiber metrics, including PSR area, count, width, and length, were measured using PSR staining. The images for collagen fiber metrics were acquired using a confocal microscope (Zeiss LSM 700, Carl Zeiss Meditec, Oberkochen,

Germany), visualized using the ZEN program (Carl Zeiss Meditec), and then measured using CT-FIRE fiber detection software (LOCI, Madison, Wisconsin, USA) [28,29].

The number of apoptotic cells was counted using automatic cell counting at 100× magnification in an average of four sections per TdT-DAB staining (TUNEL, TREVIGEN 4810-30-k).

8. Western blot analysis

The abdominal aortas were used for the western blotting assay. All samples were homogenized in RIPA lysis buffer (Bylabs, R0146CD) containing an EDTA-free protease inhibitor cocktail and centrifuged at 13,000 rpm for 10 min at 4 °C. The supernatants were collected, and the total protein content was measured using the Pierce BCA protein assay kit protocol (Thermo Scientific, Ref. 23227). The protein samples were then separated with sodium dodecyl sulfate-polyacrylamide gel electrophoresis and transferred to polyvinylidene fluoride membranes (Bio-RAD, HC, USA). After 24 h of blocking with 5% non-fat milk in Tris-buffered saline with Tween 20 (TTBS), the membrane was incubated overnight at 4 °C with primary antibodies followed by 1 h with secondary antibodies in TTBS. Most primary antibodies were used at 1:1000 dilutions, except β-actin (1:10000), while horseradish peroxidase (HRP)-conjugated goat anti-rabbit IgG (H+L) and HRP-conjugated goat anti-mouse IgG were used as secondary antibodies at a dilution of 1:5000. Protein bands were detected using West-Q Pico Dura ECL Solution and Femto ECL Solution (GenDEPOT, Houston, TX, USA). (Table 1)

Table 1. List of antibodies for western blot

Antibodies	Source	Identifier	Dilution
PCNA	Abcam	Cat#ab19166	1:1,000
α-Smooth muscle actin	Cell Signaling Technology	Cat#19245S	
TGFβ1 (Y369)	Bioworld Technology, Inc.	Cat#BS1361	
Collagen I	GeneTex	Cat#GTX26308	
Collagen III	Abcam	Cat#ab6310	
YAP1	Santa Cruz	Cat#sc-271134	
RhoA (26C4)	Santa Cruz	Cat#sc-418	
LC3B	Abcam	Cat#ab48394	
SQSTM1/p62 (D-3)	Santa Cruz	Cat#cs-28359	
mTOR (30)	Santa Cruz	Cat#sc-517464	
Phospho-mTOR (59. Ser2448)	Santa Cruz	Cat#sc-293133	
NFkB p65 (G-5)	Santa Cruz	Cat#sc-8008	
IL-6 (E-4)	Santa Cruz	Cat#sc-28343	
ICAM-1/CD54 (G-5)	Santa Cruz	Cat#sc-8439	
β-actin	Abcam	Cat#ab8224	1:10,000
Goat anti-mouse IgG (H+L)-HRP	GenDEPOT	Cat#SA001	1:5,000
Goat anti-rabbit IgG (H+L)-HRP	GenDEPOT	Cat#SA002	

9. Statistical analysis

All data are reported as mean ± standard deviation (SD) and were analyzed using GraphPad Prism 9 (GraphPad Software, San Diego, CA, USA). Comparisons between groups were carried out using one-way analysis of variance with Tukey's multiple comparison test. Statistical significance was set at $p < 0.05$.

III. RESULTS

1. Fabrication and controlled drug delivery of MN devices

A 2 × 4 array of silk MNs, which consisted of dip-coated 1 μg of sirolimus and embedded 2 μg of rosuvastatin, were structured and attached to the silk film using a transfer molding method. Figure. 2A show the array and surface of silk MNs on the silk film, which were confirmed by optical and SEM images. The results revealed that the MNs did not fall off the device 28 d after application to the rabbit abdominal aorta and remained stable. (Figure 3).

MN devices were applied to the abdominal aorta for 28 d to confirm sequential drug delivery by the MN device *in vivo*, as shown in Figure 2B. LC–MS/MS analysis was used to determine the concentrations of sirolimus and rosuvastatin in the abdominal aorta and whole blood, and their drug concentration-time profiles are shown in Figs. 2B and C. Concentrations of sirolimus and rosuvastatin in the blood and abdominal aorta were determined at various time intervals. In the abdominal aorta, the peak concentrations of sirolimus were achieved after 7 d of application, followed by a rapid decrease on day 7. In contrast, the concentration of rosuvastatin gradually increased for 28 d and reached the maximum concentration. The concentrations of sirolimus and rosuvastatin in the whole blood were not significantly different in any of the samples. Thus, sequential MN drug devices can safely deliver drugs to local tissues without being released into the blood.

In addition, we confirmed drug absorption in local lesions except for systemic diffusion through pathological analysis of organs including liver, kidney, and skeletal muscle. There were no centralized nuclei of myofibers with stain-associated myopathy. And inflammatory cells, necrosis were no present in liver and kidney tissues. (Figure 4.)

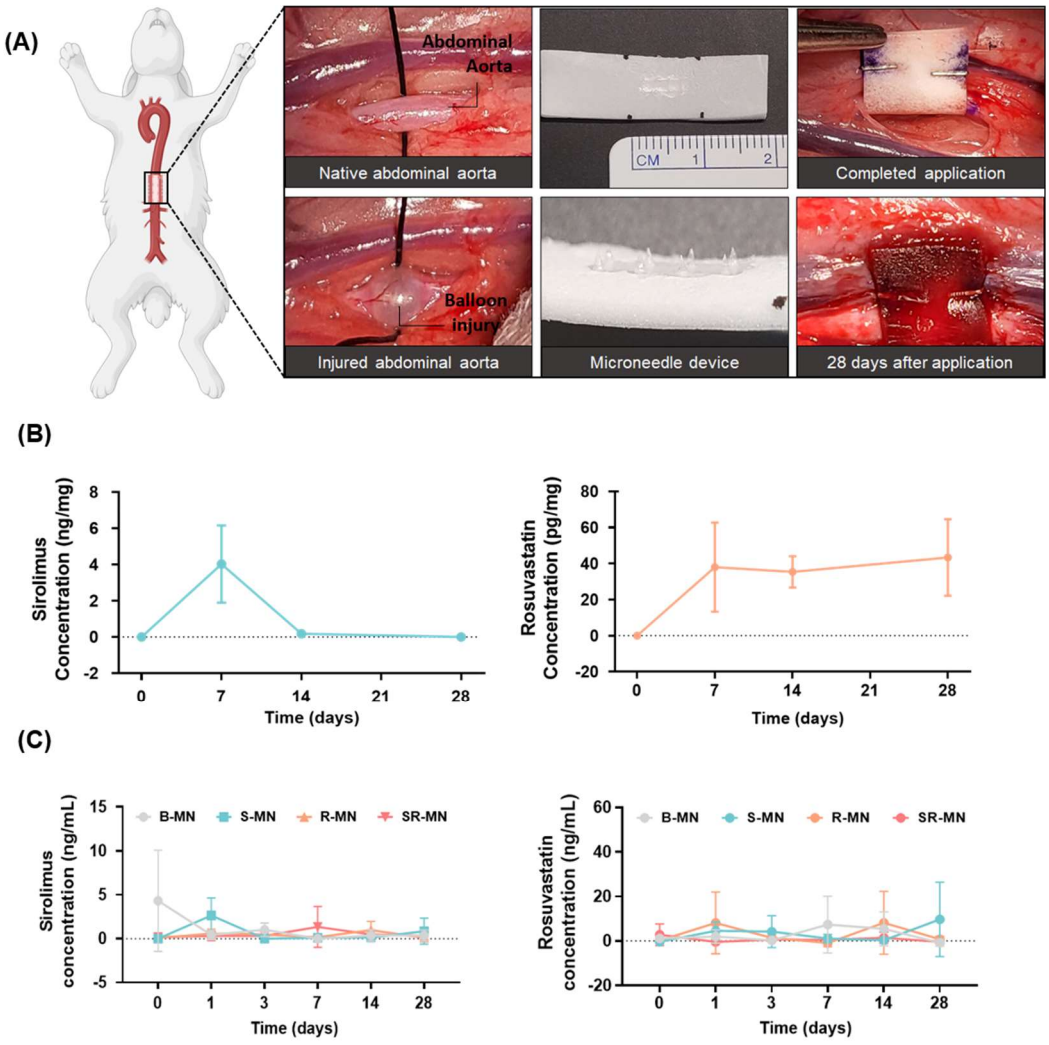

Figure 2. legend (the following page)

Figure 2. *In vivo* installation of silk-fibroin microneedle devices and the confirmed sequential drug delivery. (A) Application of SF-MN on the balloon-injured rabbit abdominal aorta. (B) Concentration of sirolimus and rosuvastatin in the abdominal aortic tissue after applying MN in rabbit (mean ± standard deviation (SD), n = 5). (C) Plasma concentration-time profiles of sirolimus and rosuvastatin after applying MN in rabbit (mean ± SD, n = 5).

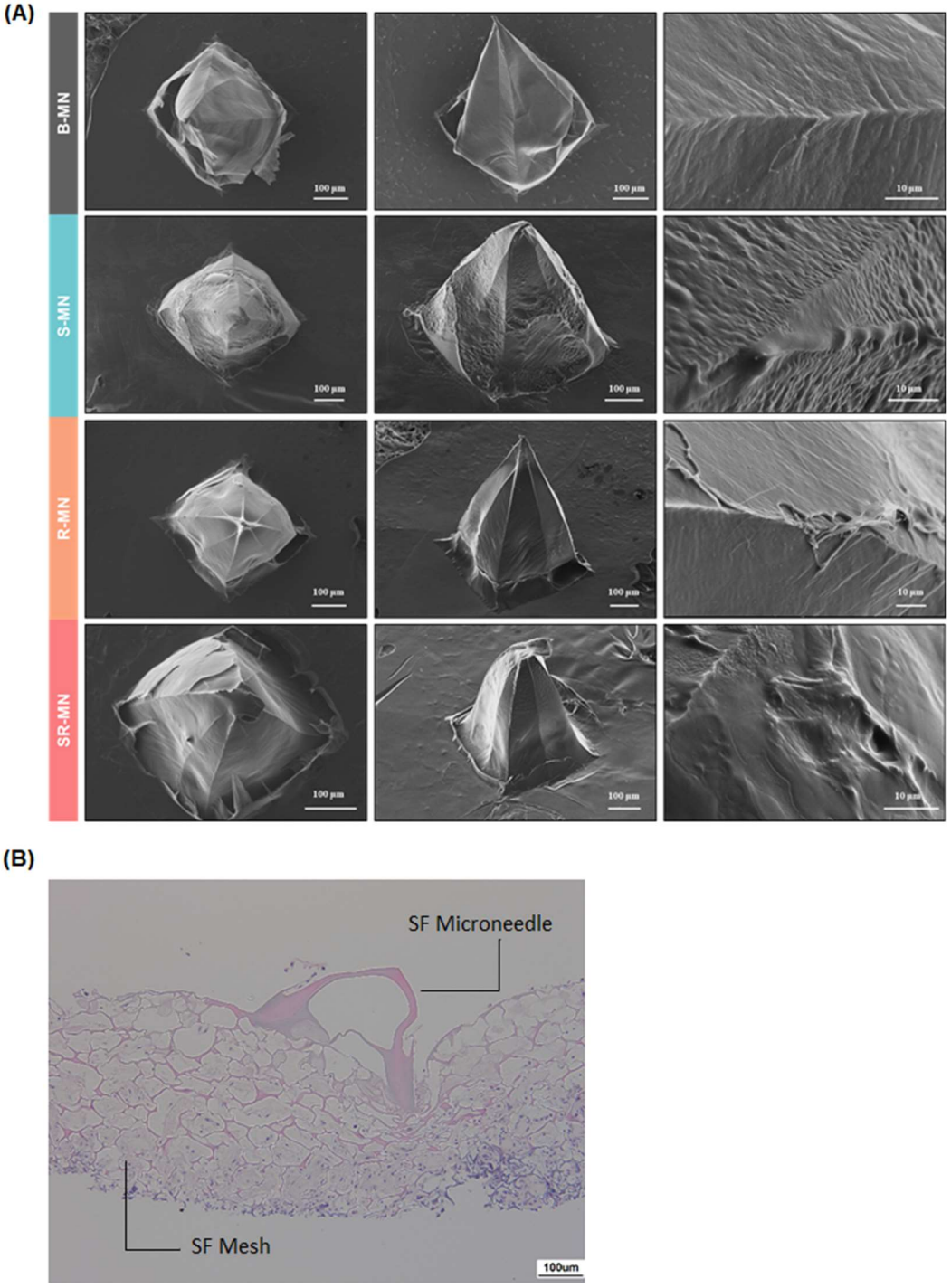

Figure 3. legend (the following page)

Figure 3. Confirmed of the silk fibroin (SF) microneedle (MN) devices. (A) Scanning electron microscopy images of the MN surfaces (Scale: 100 μm and 10 μm). (B) Hematoxylin and eosin H&E image of the silk fibroin MN 28 d after implantation (Scale: 100 μm).

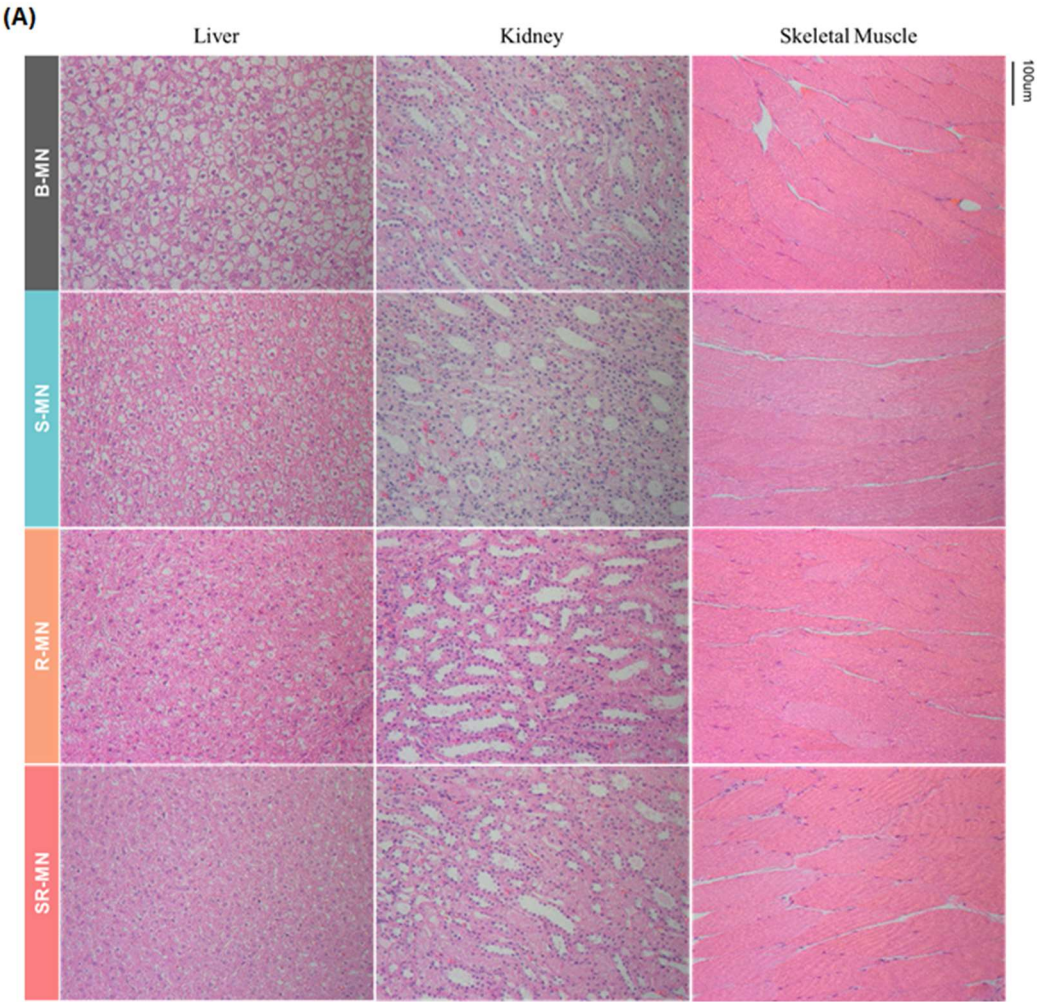

Figure 4. Safety through drug absorption in local lesions except for systemic diffusion. (A) H&E images of the major organs harvested from injured rabbit treated with drug-containing MN. (Scale: 100).

2. *In vitro* and *in vivo* biocompatibility of MN devices

Biocompatibility is a main criterion for demonstrating its use in medical devices for cardiovascular diseases. Hence, platelet adhesion tests, hemolysis, and H&E staining were performed to evaluate the blood and tissue compatibility of the MN devices. As shown in Figure 5A, platelets were rarely observed on the surface of the MN devices, and a similar number of adhered platelets was observed in all the samples. Hemolysis rates were less than 2% regardless of drug loading, indicating that the chemical safety criterion of 5% did not increase (Figure 5B). In addition, histocompatibility analysis was performed based on the low cytotoxicity and high cell viability of the MN device, as verified in a previous study[25]. Sham interventions and product applications were used to analyze the histocompatibility of the drug delivery system, excluding collateral effects such as anesthesia, surgical trauma, and postoperative management. As shown in Figure 5C, the MN device was applied to the carotid artery for tissue compatibility analysis, and morphological changes, such as inflammation and collagen, were confirmed after 28 d. No histological changes were observed in the surface and structural carotid arteries compared to those in the sham and control groups within 4 weeks.

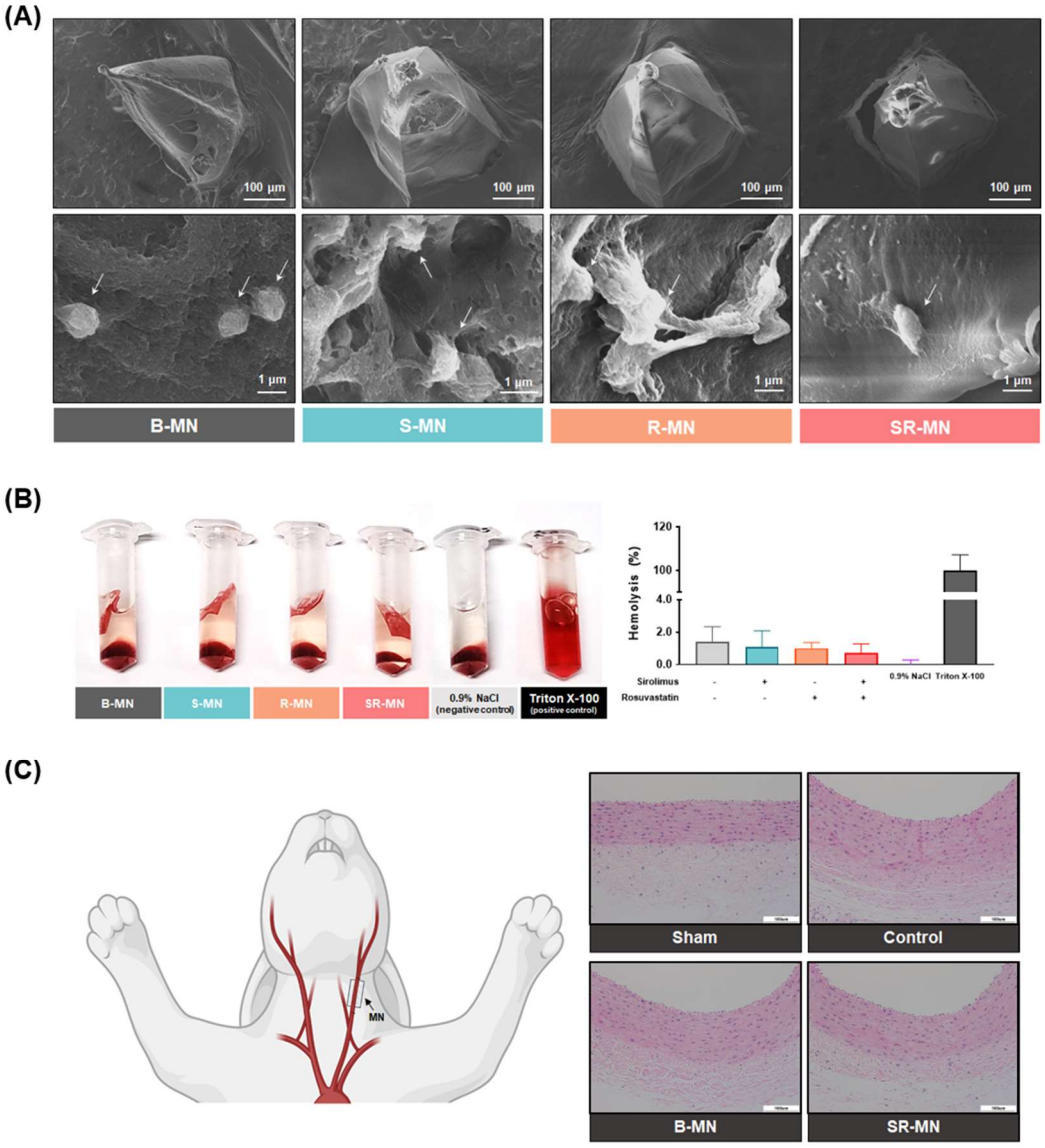

Figure 5. legend (the following page)

Figure 5. Biocompatibility assessment of the silk-fibroin microneedle devices (MN). (A) Scanning electron microscopy images of adhered platelets on MN surfaces. White arrows indicate adhered platelets (Scale: 100 μm and 1 μm). (B) Hemolytic ability of MN; appropriate quantities of 0.9% NaCl and Triton X-1000 were used as the controls; values are mean ± SD (n = 3). (C) Schematics of the *in vivo* test for tissue compatibility and hematoxylin and eosin (H&E) images of the tissue-implanted MN (n = 12; Scale: 100 μm).

3. Reduction of NI formation and IEL defect

We performed *in vivo* studies in four groups using an IH-induced rabbit model through denudation of the endothelium for 4 weeks and comparatively analyzed the B-MN and injury (injury only, N = 5) groups to confirm whether the B-MN group was suitable as a control group. The evaluation of the histological change during 2–4 weeks revealed that the NI formation and NI/media ratio were similar in both groups (Figure 6 A and 6B). Using H&E images, a significant therapeutic effect was observed in the NI formation (13.13 ± 11.17%), NI/media ratio (26.45 ± 9.28%), and adventitia/media ratio (121.33 ± 10.75%) in the case of the SR-MN group than that in the B-MN group (Figs. 7A and 7B). In particular, the amount of proliferation in the whole layer of vessels, including the intimal, medial, and adventitial layers, was lower in sirolimus release than that in strains. The elastin fiber disruption was significantly reduced in the drug-containing MN groups (S-MN group: 14.56 ± 4.23%; R-MN group: 14.50 ± 7.31%; and SR-MN group: 13.13 ± 6.3%) compared to that in the B-MN group (35.29 ± 18.64%).

Additionally, protein expressions of proliferating cell nuclear antigen (PCNA) and α-smooth muscle actin (α-SMA) were measured and quantified by the western blot analysis to examine the underlying mechanism of the effect of MN devices on VSMC proliferation induced by balloon injury, as shown in Figure 7C. The relative protein expression levels of PCNA and α-SMA were not significantly different. However, the relative protein expression level of PCNA tended to be lower in the S-MN and SR-MN groups than in the

B-MN group. In agreement with the histological results, the protein expression of PCNA showed the same trend as their respective H&E counterparts.

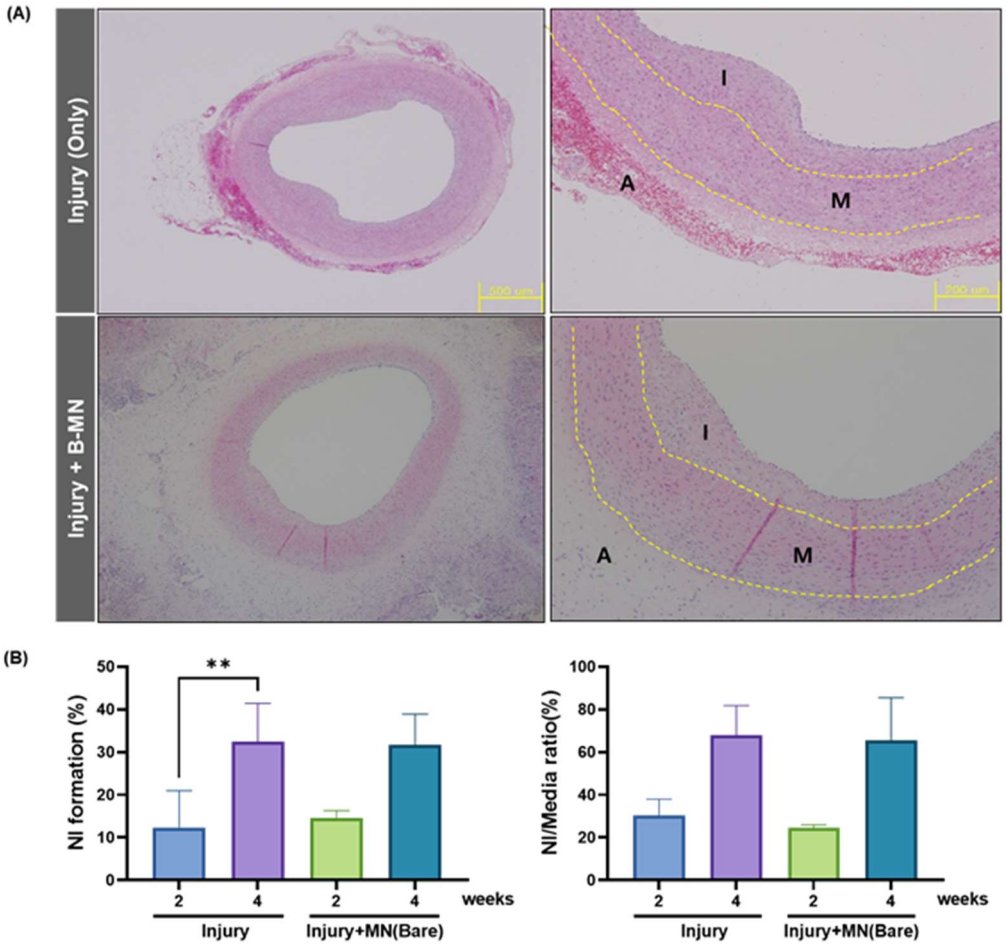

Figure 6. Comparative animal study to identify the bare-MN group as the control group. (A) H&E images of the injured rabbit abdominal aorta and SF-MN application change from 2 to 4 weeks (Scale: 500 μm and 200 μm). (B) Quantitative analysis of amount of NI formation, NI/media ratio. (**<0.01). I: tunica intima; M: tunica media; A: tunica adventitia.

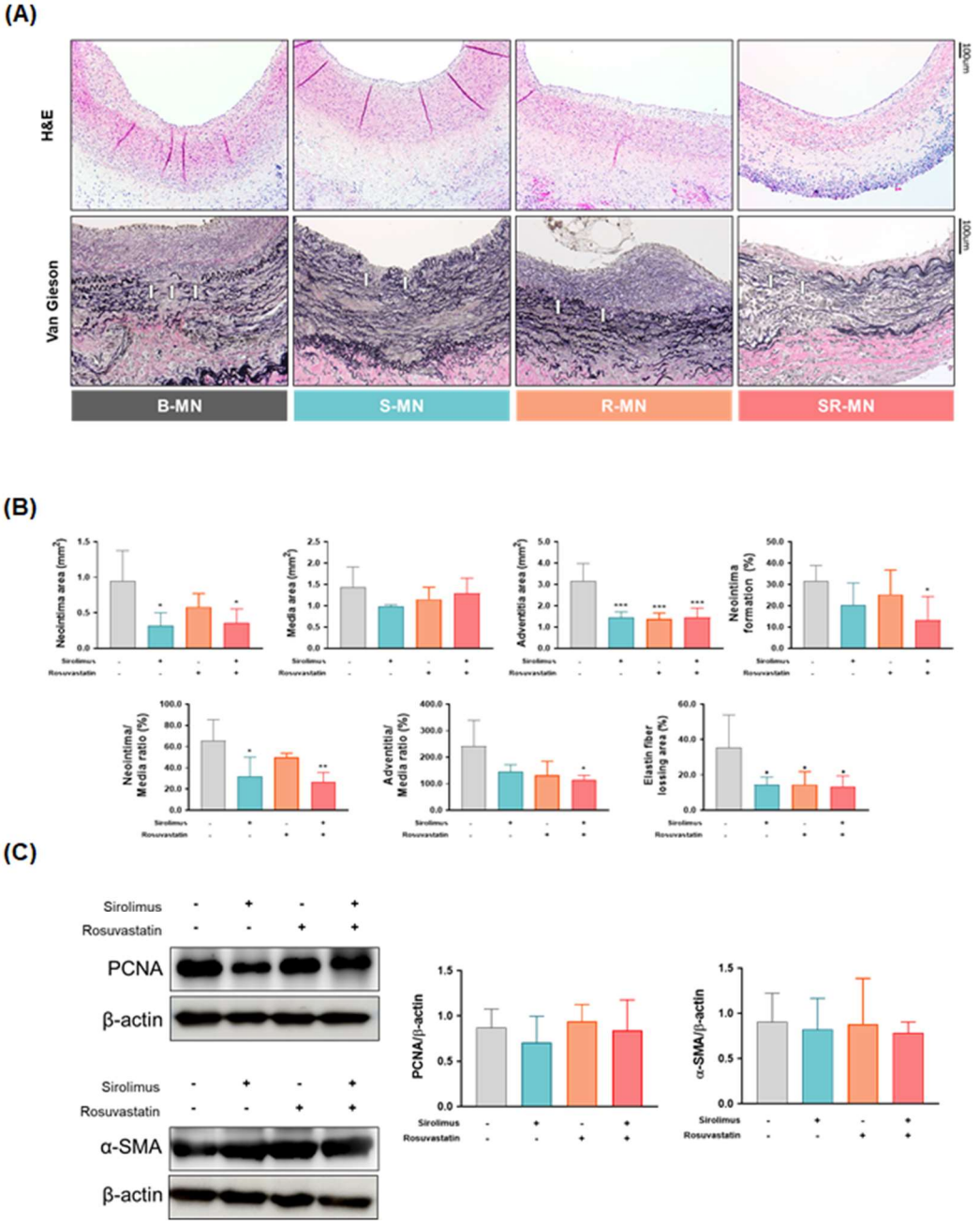

Figure 7. legend (the following page)

Figure 7. Comparative animal study of drug delivery efficacy for intimal hyperplasia reduction. (A) H&E and Van Gieson images of the SF-MN-applied abdominal aorta of the rabbit after a 4-week follow-up (Scale: 100 μm). White arrows indicate disrupted internal elastic lamina. (B) Quantitative analysis of the amount of proliferation in the whole layer of vessels (intima, media, and adventitia), NI formation, NI/media ratio, adventitia/media ratio, and elastin fiber losing area (*<0.05, **<0.01, and ***<0.001). (C) Protein expression of proliferating cell nuclear antigen (PCNA) and α-smooth muscle actin (α-SMA) as detected by the western blot.

4. Attenuated balloon injury-induced vascular fibrosis via inhibition of TGF-β pathway

To identify the potential effect of the MN devices on vascular fibrosis, we first measured the collagen density in each layer of the vessels using Masson's trichrome stain. As shown in Figs. 8A and 8B, the collagen density significantly reduced in the drug-containing MN groups (S-MN group: 99.47 ± 9.70%; R-MN group: 107.70 ± 15.97%; and SR-MN group: 96.78 ± 12.98%) compared to that in the B-MN group in the adventitial layer (121.70 ± 6.90%). In the intimal and medial layers, a significant reduction in collagen density was observed in the S-MN and SR-MN groups containing sirolimus.

In the chronic stage of IH and vascular fibrosis, the ECM accumulates and occupies most of the neointimal volume. Collagen fibers are a major component of this ECM. Accordingly, we analyzed the collagen fiber metrics (count, width, and length) in the intima layer of the MN device groups using PSR staining and CT-FIRE analysis (Figs. 9A and 9B). The PSR area and number of collagen fibers were observed to have significantly decreased in the SR-MN group (33.09 ± 7.24% and 140.89 ± 81.60, respectively) compared to that in the B-MN group (40.84 ± 10.33% and 212.38 ± 66.69, respectively). In addition, no significant difference was observed in the length of the collagen fibers between groups. However, a statistically significant decrease in the width of collagen fibers in the drug-containing MN groups (S-MN group: 6.72 ± 0.36 px; R-MN group; 6.69 ± 0.32 px; and SR-MN group: 6.74 ± 0.27 px) was observed compared to that in the B-MN groups (7.05 ± 0.32 px).

Finally, we investigated whether the changes in collagen deposition were related to the transforming growth factor- β (TGF-β) pathway (Figure 8C). The relative protein expression levels of collagen I, and collagen III decreased in the drug-containing groups compared to those in the B-MN group. particular, the collagen III protein levels in the sirolimus-containing group further decreased, and the ratio of collagen I to collagen III was higher. The relative protein expression levels of TGF-β in the SR-MN group was significant decreased compared to the B-MN group.

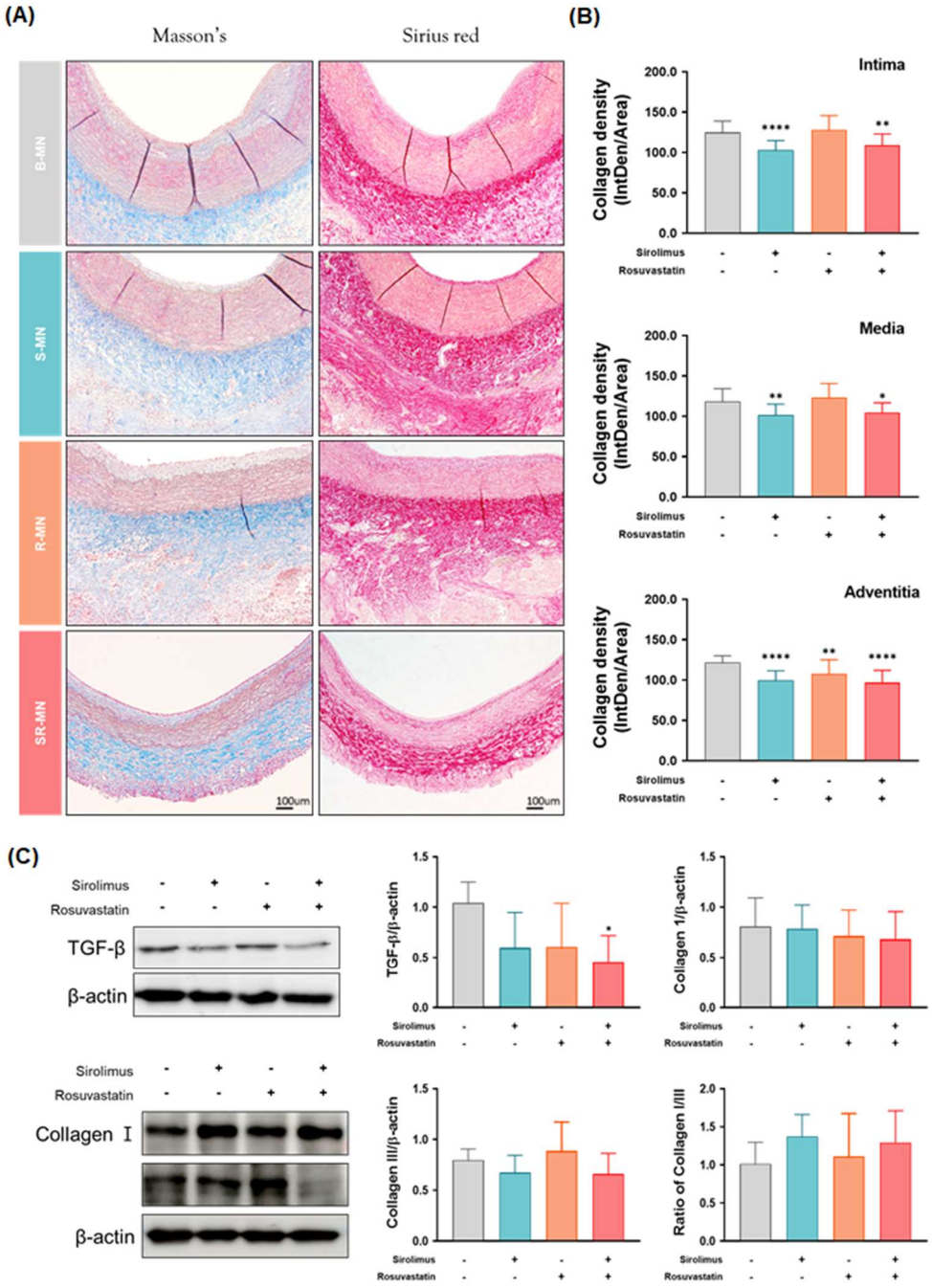

Figure 8. legend (the following page)

Figure 8. Comparative animal study of drug delivery efficacy for vascular fibrosis. (A) Masson's trichrome and Sirius red images of SF-MN-applied abdominal aorta of the rabbit applied SF-MN after 4-week follow-up (Scale: 100 μm). (B) Quantitative analysis of the collagen density in the whole layer (intima, media, and adventitia). (C) Protein expressions of TGF-β, collagen I, and collagen III as detected by the western blot. (*<0.05, **<0.01, ***<0.001, and ****<0.0001).

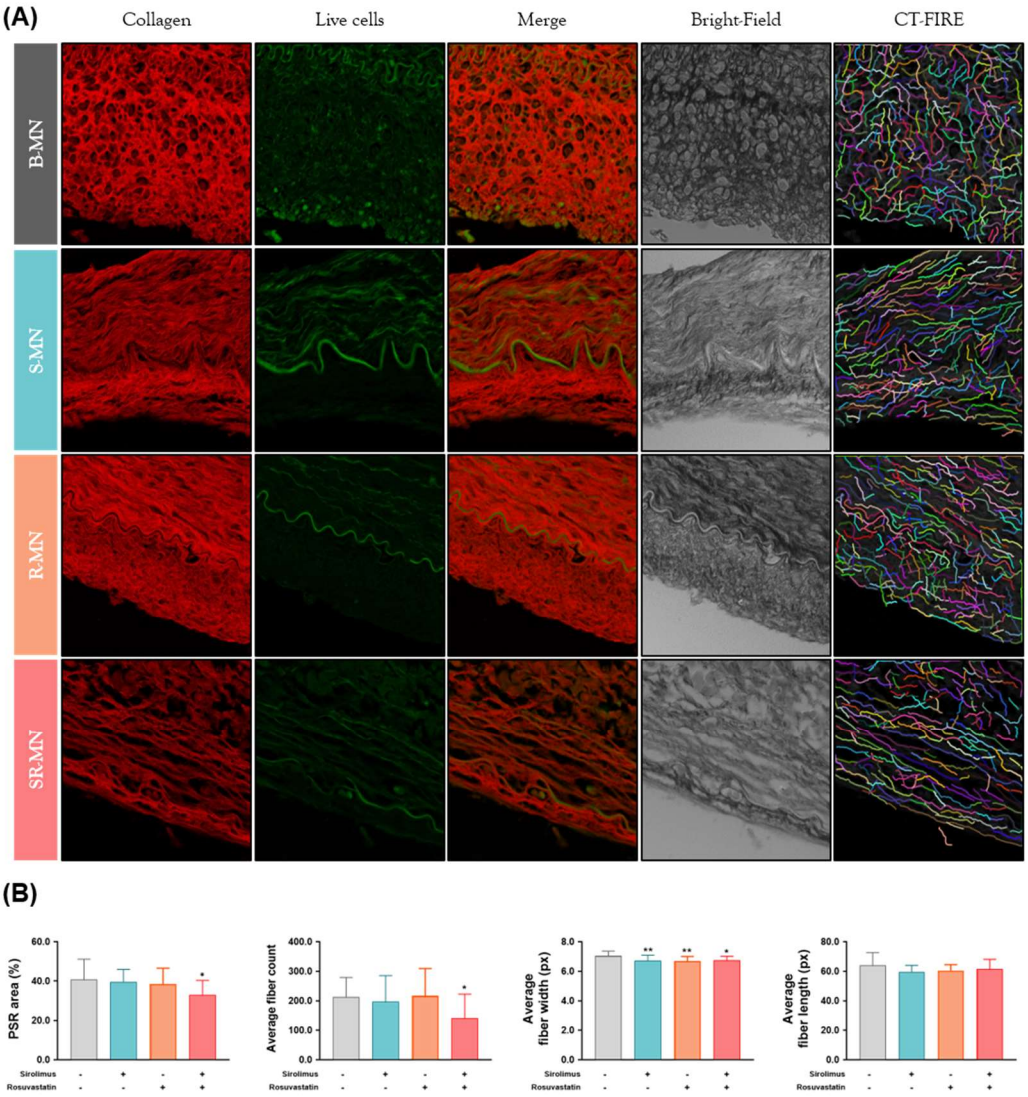

Figure 9. Comparative animal study of drug delivery efficacy for the collagen fiber metrics in the intima layer using CT-FIRE analysis. (A) Fluorescent picrosirius red (PSR) images and CT-FIRE fiber quantification software. (B) Quantitative analysis of the PSR area and collagen fiber metrics (count, width, and length) in the intimal layer. (*<0.05, **<0.01) .

5. Ameliorated vascular stiffness and remodeling through Yes-associated protein (YAP) inactivation

Ultrasonography shows excellent resolution for distinguishing between vessel wall morphology and vasoconstriction. Because the arterial stiffness and remodeling was induced by mechanical damage in the rabbit injury model, we observed the location, diameter, thickness, pressure gradient, and blood flow velocity before and 4 weeks after surgery (Figs. 10A and 10B). Compared to the B-MN group (4.88 ± 0.33 m/s and 63.10 ± 0.83 cm/s, respectively), the aortic PWV and PSV dramatically decreased in the drug-containing MN groups (S-MN group: 1.80 ± 0.26 m/s and 50.10 ± 9.26 cm/s; R-MN group: 2.14 ± 0.29 m/s and 43.38 ± 5.50 cm/s and SR-MN group: 2.34 ± 0.31 m/s and 46.69 ± 5.49 cm/s, respectively). Conversely, the Circ strain increased in the drug-containing MN groups, with significant differences observed in the S-MN group (B-MN group: 3.32 ± 0.36%; S-MN group: 14.92 ± 4.30%; R-MN group: 8.24 ± 1.54%; SR-MN group: 7.97 ± 2.14%). We also confirmed that the aortic PI among the aortic function indices significantly decreased in the R-MN group (2.89 ± 0.42) compared to that in the S-MN group (3.95 ± 1.20) (Figure 10C).

We also confirmed that DC and CC, which measure the ability of arteries to expand and the ratio of change in volume in response to pulse pressure, increased in drug-containing MN groups compared to that in the B-MN group. The Young's modulus, which is defined as the modulus of elasticity, was also observed to have decreased significantly in the drug-containing MN groups (S-MN group: 0.06 ± 0.04 MPa; R-MN group: 0.05 ± 0.03 MPa;

and SR-MN group: 0.06 ± 0.02 MPa) compared to that in the B-MN group (0.22 ± 0.13 MPa) (Figure 10C).

Yes-associated protein (YAP) activation mediates arterial stiffness via the TGF-β pathway. To determine whether vascular stiffness and remodeling were reversed through YAP inactivation, we assessed the relative protein expression levels of YAP and RhoA, an upstream regulator of YAP and a major stiffness signal transmitter. Application of MN devices containing sirolimus and rosuvastatin (S-MN group or/and R-MN group) decreased the expressions of RhoA and YAP1 compared to the B-MN group. Furthermore, the MN devices containing sirolimus and rosuvastatin (SR-MN group) exhibited additive effects (Figure 10D).

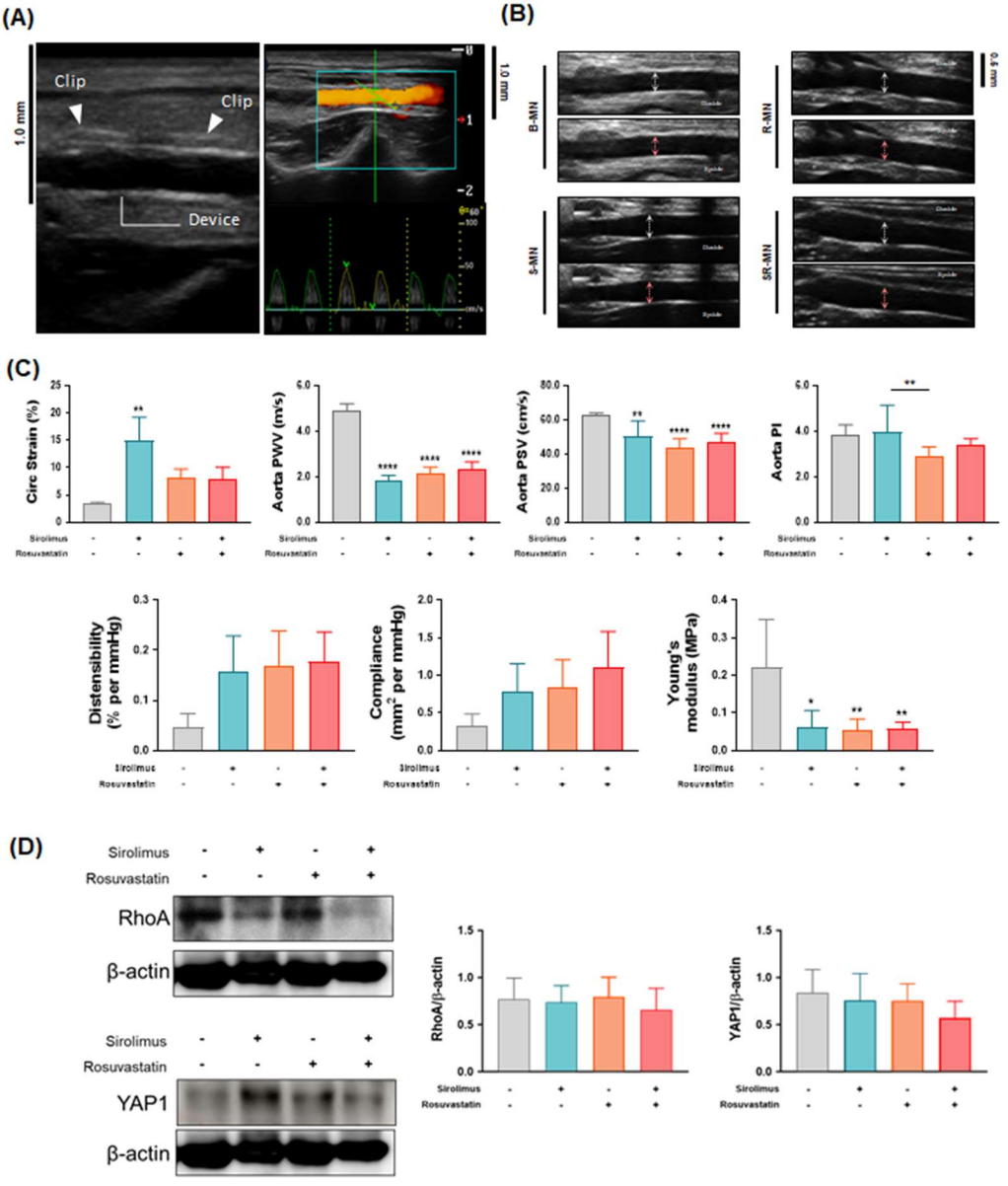

Figure 10. legend (the following page)

Figure 10. Comparative animal study of drug delivery efficacy for arterial stiffness via non-invasive sonography. (A) Sonographic images of the sagittal view and color Doppler of the abdominal aorta applied in the device. (B) Sonographic images of the abdominal aorta at the systole and diastole to evaluate arterial stiffness. (C) Quantitative analysis of aortic stiffness by Circ strain, aortic pulse wave velocity (PWV), aortic pulse systolic velocity (PSV), aortic pulsatility index (PI), distensibility, compliance, and Young's modulus (D) Protein expression of RhoA and YAP1 as detected by the western blot. (*<0.05, **<0.01, and ****<0.0001).

6. Inhibition of balloon injury-induced medial SMC apoptosis via mTOR/nuclear factor kappa B (NF-κB) signaling pathway

Vascular stress, such as stretching of the medial SMC after balloon injury, can lead to intimal proliferation and the rapid onset of apoptosis. The previous results indicated that inactivated YAP was involved in cell survival, proliferation, and apoptosis. In agreement with YAP protein expression results, the TUNEL assay results showed that apoptotic cells reduced in drug-containing MN groups (S-MN group: 294.40 ± 186.40; R-MN group: 200.05 ± 93.07; and SR-MN group: 167.25 ± 28.63) compared to the B-MN group (528.00 ± 270.74), and the rosuvastatin-containing groups particularly showed a remarkable difference (Figure 11A).

Western blot analysis was performed to understand the apoptosis inhibition function of the drug-containing MN devices by considering the mechanism of action of sirolimus and rosuvastatin, which are mTOR and HMG-CoA inhibitors, respectively. All drug-containing MN groups showed reduced mTOR phosphorylation compared to the B-MN group. Nuclear factor kappa B (NF-κB), which is controlled by mTOR downstream targets, is a key transcription factor that regulates proliferation, inflammatory responses, and autophagy. Consistent with the results of mTOR inactivation, the relative protein expression levels of NF-κB decreased in the drug-containing MN groups compared to that in the B-MN group; however, a significant difference was observed in the SR-MN group (Figure 11B).

Next, we evaluated whether NF-κB reduction by drug-containing MN affected the expression of NF-κB target genes. We found that SR-MN significantly decreased the level of ICAM-1 protein and decreased the levels of IL-6 and SQTM1/p62 (Figure 11C).

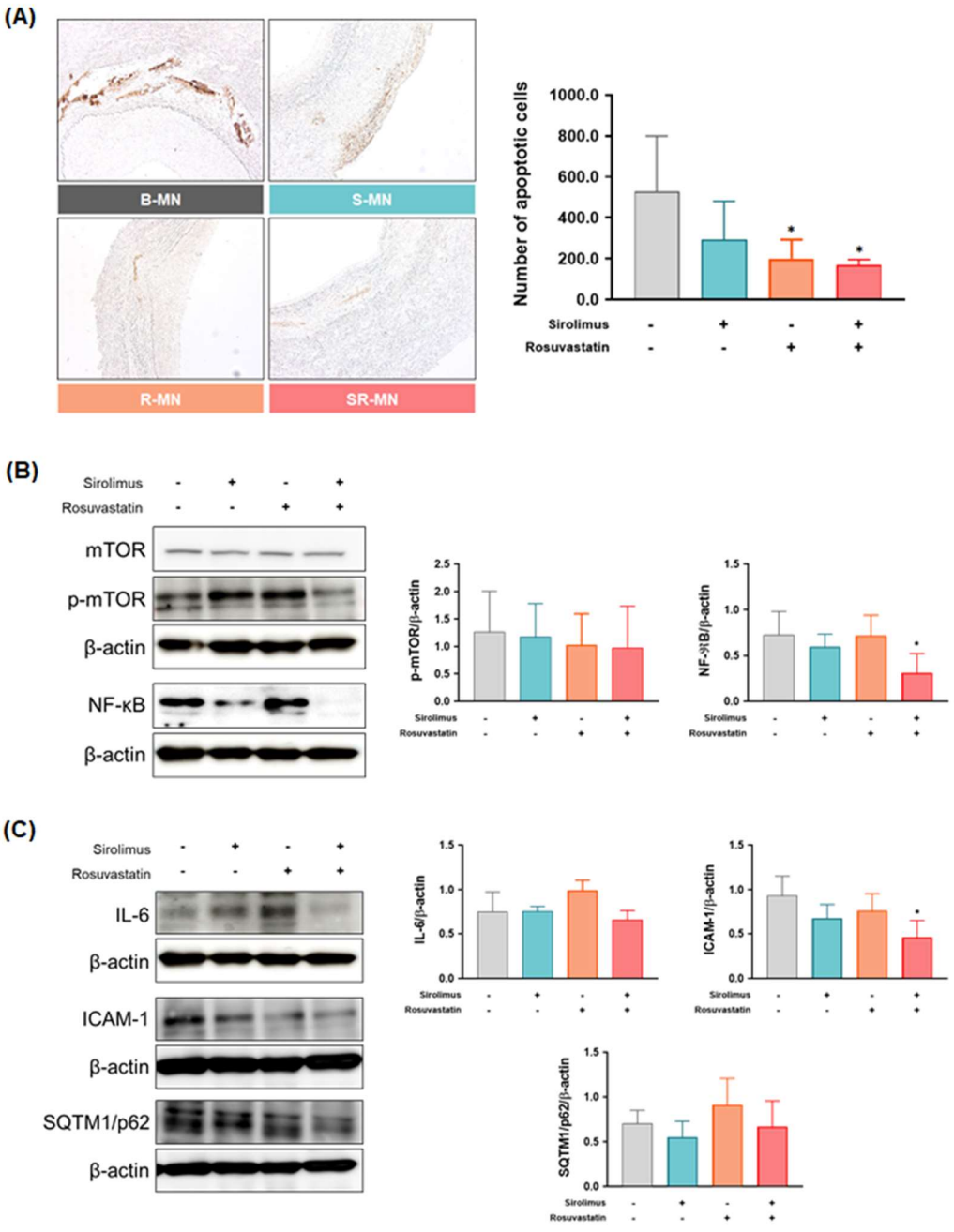

Figure 11. legend (the following page)

Figure 11. Comparative animal study of drug delivery efficacy to inhibit apoptosis in vascular smooth muscle cells (VSMCs) via mechanistic target of rapamycin (mTOR)/ nuclear factor kappa B (NF-kB) signaling pathway. (A) TUNEL images of the SF-MN-applied abdominal aorta of a rabbit after a 4-week follow-up, and quantitative analysis of apoptotic cells (Scale: 500 μm). (B) Protein expression of mTOR, p-mTOR, and NF-κB detected by the western blot. (C) Protein expression of IL-6, ICAM-1, and SQTM1/p62 detected by the western blot (*<0.05).

IV. DISCUSSION

Vascular restenosis with IH is an excessive wound-healing reaction of the vessels that occurs in vascular revascularization procedures, such as percutaneous transluminal angioplasty, stent implantation, and bypass grafting [3,4]. The leading cause of IH is endothelial damage, which is unavoidable in all vascular regeneration procedures. This process develops over time from the acute to chronic phase; the platelets aggregate and adhere to the injured endothelial lesion, releasing mitogenic growth factors to attract macrophages and VSMCs to switch their phenotype to synthetic. Growth factors and inflammatory mediators induce synthetic proliferation of VSMCs, secretion of ECM components, and migration into the subintimal space. The neointima, which is mostly composed of the resynthesized ECM, is then clearly thickened. Myofibroblasts are derived from the cytokine TGF-β, a major biochemical inducer of myofibroblast differentiation, which is generated under mechanical and biochemical stimuli [8,10]. Although myofibroblasts can be derived from adventitial fibroblasts, they can also be derived from the transdifferentiation of SMCs in the tunica media and endothelial cells.

Moreover, depending on the degree of damage, the activated myofibroblasts either undergo apoptosis or survive, contributing to vascular fibrosis and remodeling [30]. In addition, biophysical signals such as compressive and tensile forces play important roles in vascular healing, such as controlling transcriptional programs for cell proliferation, differentiation, and transformation. An increase in ECM stiffness results in the nuclear

translocation of YAP/TAZ to regulate cell growth migration and differentiation, sense ECM stiffness through local adhesion, and promote stress fiber formation [31,32].

By understanding these multifactorial properties, we developed a microneedle-based outer-wall device that induces the short- and long-term release of sirolimus (an mTOR inhibitor) and rosuvastatin (an HMG-CoA inhibitor), respectively, as a therapeutic strategy. In addition, according to our previous studies, the drug release rate was successfully controlled by a dip-coating method using 50/50 PLGA with a fast degradation rate as a drug delivery carrier [33] and an eluting method using silk fibroin with a longer degradation rate as a carrier [25]. As shown *in vivo* through the abdominal aortic injury model (Figure 2), the reduced collagen density, fibrosis, and TGF-β expression in the SR-MN group were found to be remarkable, suggesting a synergistic effect of the inhibition of the TGF-β pathway through sequential drug release (Figure 8).

Additionally, consistent with the results of the reduction of vascular fibers, which are the main component of the hyperproliferated intima, the inhibitory effect of the initially released sirolimus on intimal proliferation, and the inhibitory effect on intima and adventitia through the sequential release of the two drugs were confirmed (Figure 8-9). In addition, regarding the inactivation of RhoA and YAP through the sequential release of drugs, significant reductions were observed in aortic PWV and PSV (representative indicators of arterial stiffness) and Young's modulus (an indicator of vascular electricity) (Figure 10)[34].

In particular, the activation of YAP mediated arterial stiffness via the TGF-β pathway, which is caused by inducing TGF-β inhibition through the intervention of sirolimus and rosuvastatin from the acute to chronic phase in an IH process. Furthermore, the strategic mediation of the mTOR/NF-kB signaling pathway through the sequential release of sirolimus and rosuvastatin decreased levels of VCAM-1 and IL-6, which are major players in IH progression, and reduced apoptosis through autophagy induction. Consistent with the TUNEL assay results, the apoptotic cells significantly reduced in the drug-containing MN device, which was interpreted as a result of SMC apoptosis in the medial through the mediation of the mTOR/NF-κB pathway [35].

Our study showed that the drug released through an external vascular device with microneedles was sufficiently absorbed into the localized lesion, except for systemic diffusion, preventing vascular restenosis without affecting organs. (Figure 4).

However, these results were observed on day 28, and longer follow-up results, including peak value and extinction period of drugs and IH progression *in vivo*, are required for clinical trials. In addition, most patients with coronary artery disease belong to a high-risk group with underlying diseases, such as diabetes, hypert1ension, and hyperlipidemia, and have uncomplicated lesions [36,37]. Therefore, further studies are essential for evaluation and analysis via the application of high-risk models and complex lesions, which will be a promising strategy in clinical practice. Furthermore, the long-term release of the target drug can be sufficiently controlled by the degree of density of silk fibroin as a drug delivery carrier, which can be an efficient treatment strategy for coronary artery disease and surgical

vascular access, such as peripheral vascular disease and arteriovenous fistulas in renal dialysis patients [38].

V. CONCLUSION

The perivascular device is a promising approach for intensive drug delivery to the lesion after bypass surgery, and the sequential release of sirolimus and rosuvastatin, which reflects the pathophysiology of restenosis, can be a useful treatment strategy in clinical practice.

REFERENCES

1 Patel, M. R. *et al.* ACC/AATS/AHA/ASE/ASNC/SCAI/SCCT/STS 2017 Appropriate Use Criteria for Coronary Revascularization in Patients With Stable Ischemic Heart Disease: A Report of the American College of Cardiology Appropriate Use Criteria Task Force, American Association for Thoracic Surgery, American Heart Association, American Society of Echocardiography, American Society of Nuclear Cardiology, Society for Cardiovascular Angiography and Interventions, Society of Cardiovascular Computed Tomography, and Society of Thoracic Surgeons. *Journal of the American College of Cardiology* **69**, 2212-2241, doi:https://doi.org/10.1016/j.jacc.2017.02.001 (2017).

2 Fihn Stephan, D. *et al.* 2014 ACC/AHA/AATS/PCNA/SCAI/STS Focused Update of the Guideline for the Diagnosis and Management of Patients With Stable Ischemic Heart Disease. *Journal of the American College of Cardiology* **64**, 1929-1949, doi:10.1016/j.jacc.2014.07.017 (2014).

3 Buszman, P. E. *et al.* Left Main Stenting in Comparison With Surgical Revascularization: 10-Year Outcomes of the (Left Main Coronary Artery Stenting) LE MANS Trial. *JACC Cardiovasc Interv* **9**, 318-327, doi:10.1016/j.jcin.2015.10.044 (2016).

4 Buszman, P. E. *et al.* Early and long-term results of unprotected left main coronary artery stenting: the LE MANS (Left Main Coronary Artery Stenting) registry. *J Am Coll Cardiol* **54**, 1500-1511, doi:10.1016/j.jacc.2009.07.007 (2009).

5 Owens, C. D., Gasper, W. J., Rahman, A. S. & Conte, M. S. Vein graft failure. *Journal of vascular surgery* **61**, 203-216 (2015).

6 Mylonaki, I. *et al.* Perivascular medical devices and drug delivery systems: Making the right choices. *Biomaterials* **128**, 56-68, doi:https://doi.org/10.1016/j.biomaterials.2017.02.028 (2017).

7 Rajagopal, V. & Rockson, S. G. Coronary restenosis: a review of mechanisms and management. *Am J Med* **115**, 547-553, doi:10.1016/s0002-9343(03)00477-7 (2003).

8 Melnik, T., Jordan, O., Corpataux, J.-M., Delie, F. & Saucy, F. Pharmacological prevention of intimal hyperplasia: A state-of-the-art review. *Pharmacology & Therapeutics* **235**, 108157, doi:https://doi.org/10.1016/j.pharmthera.2022.108157 (2022).

9 Li, Y. *et al.* Biodegradable Magnesium Alloy Stents as a Treatment for Vein Graft Restenosis. *Yonsei Med J* **60**, 429-439 (2019).

10 Forte, A., Della Corte, A., De Feo, M., Cerasuolo, F. & Cipollaro, M. Role of myofibroblasts in vascular remodelling: focus on restenosis and aneurysm. *Cardiovascular Research* **88**, 395-405, doi:10.1093/cvr/cvq224 (2010).

11 Krishnan, P. *et al.* Enhanced neointimal fibroblast, myofibroblast content and altered extracellular matrix composition: Implications in the progression of human peripheral artery restenosis. *Atherosclerosis* **251**, 226-233, doi:10.1016/j.atherosclerosis.2016.06.046 (2016).

12 Chen, G. *et al.* Unimolecular Micelle-Based Hybrid System for Perivascular Drug Delivery Produces Long-Term Efficacy for Neointima Attenuation in Rats. *Biomacromolecules* **18**, 2205-2213, doi:10.1021/acs.biomac.7b00617 (2017).

13 Yu, X. *et al.* A rapamycin-releasing perivascular polymeric sheath produces highly effective inhibition of intimal hyperplasia. *Journal of Controlled Release* **191**, 47-53, doi:https://doi.org/10.1016/j.jconrel.2014.05.017 (2014).

14 Yang, Q. *et al.* A novel biodegradable external stent regulates vein graft remodeling via the Hippo-YAP and mTOR signaling pathways. *Biomaterials* **258**, 120254, doi:https://doi.org/10.1016/j.biomaterials.2020.120254 (2020).

15 Zhang, Y. *et al.* Time-dependently slow-released multiple-drug eluting external sheath for efficient long-term inhibition of saphenous vein graft failure. *Journal of Controlled Release* **293**, 172-182, doi:https://doi.org/10.1016/j.jconrel.2018.12.001 (2019).

16 Linn, Y. L. *et al.* Utility of sirolimus coated balloons in the peripheral vasculature - a review of the current literature. *CVIR Endovasc* **5**, 29, doi:10.1186/s42155-022-00308-z (2022).

17 Linn, Y. L. *et al.* Utility of sirolimus coated balloons in the peripheral vasculature – a review of the current literature. *CVIR Endovascular* **5**, 29, doi:10.1186/s42155-022-00308-z (2022).

18 Kim, J. S. *et al.* Effect of High-Dose Statin Therapy on Drug-Eluting Stent Strut Coverage. *Arterioscler Thromb Vasc Biol* **35**, 2460-2467, doi:10.1161/atvbaha.115.306037 (2015).

19 Natsuaki, M. *et al.* Impact of Statin Therapy on Late Target Lesion Revascularization After Sirolimus-Eluting Stent Implantation (from the CREDO-Kyoto Registry Cohort-2). *The American Journal of Cardiology* **109**, 1387-1396, doi:https://doi.org/10.1016/j.amjcard.2012.01.350 (2012).

20 Asada, K. *et al.* Impact of statin therapy on late target lesion revascularization after everolimus-eluting stent implantation according to

pre-interventional vessel remodeling and vessel size of treated lesion. *Heart and Vessels*, doi:10.1007/s00380-022-02104-0 (2022).

21 Kim, G. S. *et al.* Impact of Statin Treatment Intensity after Endovascular Revascularization on Lower Extremity Peripheral Artery Disease. *Yonsei Med J* **63**, 333-341 (2022).

22 Lee, S. Y. *et al.* Statin Intensity and Clinical Outcome in Patients with Stable Coronary Artery Disease and Very Low LDL-Cholesterol. *PLOS ONE* **11**, e0166246, doi:10.1371/journal.pone.0166246 (2016).

23 Diana Hla, R. J., MD; Roger S. Blumenthal, MD, FACC; Seth Shay Martin, MD, MHS, FACC. Assessing Severity of Statin Side Effects: Fact Versus Fiction. *AMERICAN COLLEGE of CARDIOLOGY* (2018).

24 Lee, J. *et al.* Transfer-molded wrappable microneedle meshes for perivascular drug delivery. *Journal of Controlled Release* **268**, 237-246, doi:https://doi.org/10.1016/j.jconrel.2017.10.007 (2017).

25 Lee, J. *et al.* Highly flexible and porous silk fibroin microneedle wraps for perivascular drug delivery. *Journal of Controlled Release* **340**, 125-135, doi:https://doi.org/10.1016/j.jconrel.2021.10.024 (2021).

26 Seidel, S. R. T. *et al.* Does Double Centrifugation Lead to Premature Platelet Aggregation and Decreased TGF-β1 Concentrations in Equine Platelet-Rich Plasma? *Vet Sci* **6**, doi:10.3390/vetsci6030068 (2019).

27 Yang, L. *et al.* A robust mussel-inspired zwitterionic coating on biodegradable poly(L-lactide) stent with enhanced anticoagulant, anti-inflammatory, and anti-hyperplasia properties. *Chemical Engineering Journal* **427**, 130910, doi:https://doi.org/10.1016/j.cej.2021.130910 (2022).

28 Wegner, K. A., Keikhosravi, A., Eliceiri, K. W. & Vezina, C. M. Fluorescence of Picrosirius Red Multiplexed With Immunohistochemistry for the Quantitative Assessment of Collagen in Tissue Sections. *Journal of Histochemistry & Cytochemistry* **65**, 479-490, doi:10.1369/0022155417718541 (2017).

29 Vogel, B., Siebert, H., Hofmann, U. & Frantz, S. Determination of collagen content within picrosirius red stained paraffin-embedded tissue sections using fluorescence microscopy. *MethodsX* **2**, 124-134, doi:10.1016/j.mex.2015.02.007 (2015).

30 Kalluri, R. & Neilson, E. G. Epithelial-mesenchymal transition and its implications for fibrosis. *The Journal of clinical investigation* **112**, 1776-1784 (2003).

31 Cai, X., Wang, K. C. & Meng, Z. Mechanoregulation of YAP and TAZ in Cellular Homeostasis and Disease Progression. *Front Cell Dev Biol* **9**, 673599, doi:10.3389/fcell.2021.673599 (2021).

32 Stehouwer, C. D. A., Henry, R. M. A. & Ferreira, I. Arterial stiffness in diabetes and the metabolic syndrome: a pathway to cardiovascular disease. *Diabetologia* **51**, 527-539, doi:10.1007/s00125-007-0918-3 (2008).

33 Choi, C. K., Kim, J. B., Jang, E. H., Youn, Y. N. & Ryu, W. H. Curved Biodegradable Microneedles for Vascular Drug Delivery. *Small* **8**, 2483-2488, doi:10.1002/smll.201200441 (2012).

34 Messas, E., Pernot, M. & Couade, M. Arterial wall elasticity: State of the art and future prospects. *Diagnostic and Interventional Imaging* **94**, 561-569, doi:https://doi.org/10.1016/j.diii.2013.01.025 (2013).

35 Hu, M. *et al.* Substrate stiffness differentially impacts autophagy of endothelial cells and smooth muscle cells. *Bioact Mater* **6**, 1413-1422, doi:10.1016/j.bioactmat.2020.10.013 (2021).

36 Yang, Y. *et al.* A Clinical Model to Identify Patients With High-Risk Coronary Artery Disease. *JACC: Cardiovascular Imaging* **8**, 427-434, doi:https://doi.org/10.1016/j.jcmg.2014.11.015 (2015).

37 van den Berg, M. J. *et al.* Identification of vascular patients at very high risk for recurrent cardiovascular events: validation of the current ACC/AHA very high risk criteria. *European Heart Journal* **38**, 3211-3218, doi:10.1093/eurheartj/ehx102 (2017).

38 Irani, F. G. *et al.* Hemodialysis Arteriovenous Fistula and Graft Stenoses: Randomized Trial Comparing Drug-eluting Balloon Angioplasty with Conventional Angioplasty. *Radiology* **289**, 238-247, doi:10.1148/radiol.2018170806 (2018).

ABSTRACT (In Korean)

시롤리무스와 스타틴의 순차적 방출이 유도된

실크피브로인 마이크로니들을 통한 혈관내막과다증식 예방효과

<지도교수 윤 영 남>

연세대학교 대학원 생체공학협동과정

장 의 화

내막증식증은 혈관우회로술 후 혈관재협착의 주요 원인이며, 혈관우회로술 과정에서 발생되는 내피손상을 시작으로 하여 급성에서 만성의 일련의 과정으로 진행된다. 내막증식증을 예방하기 위해서는 각 단계의 주요신호전달 경로 이해를 통한 약리학적 접근이 필요하다. 특히, 내막증식증의 병태생리를 반영한 약물 접근에 있어서, 경구 또는 정맥내 주입을 통한 약물사용으로 발생하는 전신부작용을 최소화 할 수 있는 혈관 병소의 국소 약물 전달 시스템의 전략이 필요하다.

본 연구에서는 실크피브로인 기반 마이크로니들 장치를 이용하여 라파마이신 (mTOR) 억제제의 경로 표적인 시롤리무스 (sirolimus)와 HMG-CoA 억제제인 스타틴 (statin)의 순차적 방출을 생체 내 에서 성공적으로 구현하였다.

유도된 내피 손상 후 급성기에 방출된 시롤리무스는 transforming growth factor(TGF)-β / mTOR 억제를 통해 혈관 평활근 세포(VSMC) 증식과 혈관섬유증을 감소효과를 보였다. 그리고 급성에서 만성단계까지 지속적으로 방출되는 스타틴은 TGF- β / YAP 불활성화를 통해 혈관 강직과 세포사멸 감소효과를 보였다. 또한, 시롤리무스와 스타틴의 순차적 방출은 mTOR/NF-kB 경로 억제를 통해 혈관 염증, 자가포식, 세포 증식 및 세포외기질 분해 리모델링에 대한 상승적 치료효과를 보였다.

이러한 결과는 내피 손상 후 내막증식 진행과정에서 신생내막의 혈관섬유밀도의 유의한 감소와 혈관 탄성 보존으로 혈관 재협착을 예방하는 내막증식증의 치료효과를 입증하였다. 또한, 전신약물확산이 아닌 표적 병변에 약물을 국소적으로 전달하여 약물 독성으로부터 안전성이 확인되었다. 나아가 이 연구는 당뇨병, 고혈압 및 고지혈증과 같은 기저질환이 있는 환자의 맞춤형 약물 조합으로 국소적 약물 전달을 통해 관상동맥 질환을 치료하기 위한 유망한 전략의 제시를 성공적으로 검증하였다.

핵심되는 말: 내막증식증, 혈관우회로술, 마이크로니들, 실크피브로인, 국소적 약물 전달